On the Interaction of 95-Mev Protons with D, Li, Be, C, Al, Cu, and Pb Nuclei*

J. A. HOFMANN† AND K. STRAUCH‡
Harvard University, Cambridge, Massachusetts
(Received December 22, 1952)

A measurement has been made of the energy distribution of neutrons emitted from various targets at angles of 0°, 5°, 10°, 16°, and 28° with respect to the primary 95-Mev proton beam. The results fall into three groups: (1) the number of neutrons emitted by C, Al, Cu, and Pb targets decreases with neutron energy and with angle of emission; (2) the energy distribution of neutrons emitted from D is peaked, but the width is believed to represent mainly the energy distribution of the primary proton beam; (3) neutrons emitted from Li and Be show a peaked energy distribution, with the size of the peak decreasing rapidly with increasing angle of emission. The spectra obtained from the heavier elements appear to be in general agreement with the theory of high energy nuclear reactions based on the generation of a nuclear cascade. However, the forward minimum and the high energy peak predicted by Goldberger's calculations have not been observed with the heavier elements. The results obtained with Be are interpreted on the basis of a very simplified model.

I. INTRODUCTION

THE development of the synchrocyclotron has allowed studies in the laboratory of the neutron-proton and proton-proton interactions at energies of 40 Mev and above. It is disappointing that the theoretical interpretation of these experiments has not, as yet, led to a satisfactory solution of the nuclear force problem, even in such relatively simple systems.[1] In spite of this, studies of the interaction of high energy neutrons and protons with more complicated nuclei are still of considerable interest, since phenomenological interpretations of such experiments can give important information on various nuclear models.

As was first discussed by Serber,[2] the path of a high energy nucleon passing through a nucleus can be thought of as a series of nucleon-nucleon encounters which often generate a nuclear cascade. Chamberlain and Segrè[3] have recently demonstrated directly the importance of single nucleon-nucleon collisions inside a nucleus. With 345-Mev protons passing through a Li target, they have observed $p-p$ coincidence events with properties that approximate those of free collisions. This result supports the model generally used to calculate the results of the interaction of high energy particles with various nuclei. This model assumes that the nucleon-nucleon collisions inside a nucleus are "quasi-elastic." That is, the collisions have the same kinematics and scattering cross sections as free collisions, modified by the following facts: (1) since the target nucleons are bound, they have an initial momentum distribution; (2) certain collisions are forbidden by the exclusion principle and by threshold considerations.

This point of view has led to the optical model of Fernbach, Serber, and Taylor,[4,5] and the Goldberger model.[6] The optical model was devised to interpret the scattering of high-energy neutrons by various nuclei, and while quite successful around 100 Mev, it appears to be less reliable at higher energies.[5] The Goldberger model leads to detailed predictions of the energy spectrum and angular distribution of particles emitted from a nucleus when struck by a high energy nucleon. One of the purposes of the work reported here, was to test some of the predictions in the 100-Mev region.

To detect secondary particles from high energy reactions, cloud chamber,[7,8] photographic,[9–12] and counter techniques[13–18] have been used. The counter technique has the advantage that various target nuclei can be used and that good energy and angular resolution is possible. The importance of quasi-elastic collisions in the mechanism of high energy reactions is best studied by observing the angular and energy distribution of those secondary particles which have energies of the same order of magnitude as the incident nucleon. If a nearly monoenergetic particle beam is available, the momentum distribution of the quasi-elastically scattered nucleons is directly related to the momentum distribution of the nucleons inside the nucleus. In the experiment of Cladis *et al.*,[16] measurements were made of the momentum distribution of the protons scattered from D and C targets at 30° and 40° with respect to the

* Assisted by the joint program of the U. S. Office of Naval Research and U. S. Atomic Energy Commission.
† Central Scientific Company Fellow.
‡ Society of Fellows.
[1] Chamberlain, Segrè, and Wiegand, Phys. Rev. **83**, 923 (1951).
[2] R. Serber, Phys. Rev. **72**, 1114 (1947).
[3] O. Chamberlain and E. Segrè, Phys. Rev. **87**, 81 (1952).
[4] Fernbach, Serber, and Taylor, Phys. Rev. **75**, 1352 (1949).
[5] S. Fernbach, University of California Radiation Laboratory Report AEC-UCRL-1382 (unpublished).
[6] M. L. Goldberger, Phys. Rev. **74**, 1269 (1948).
[7] K. Brueckner and W. M. Powell, Phys. Rev. **75**, 1274 (1949).
[8] J. K. Bøggild and F. H. Tenney, Phys. Rev. **84**, 1070 (1951).
[9] E. W. Titterton, Phil. Mag. **42**, 109 (1951).
[10] L. S. Germain, Phys. Rev. **82**, 596 (1951).
[11] Bernardini, Booth, and Lindenbaum, Phys. Rev. **85**, 826 (1952).
[12] H. Fishman and A. M. Perry, Phys. Rev. **86**, 167 (1952).
[13] J. Hadley and H. York, Phys. Rev. **80**, 345 (1950).
[14] D. Bodansky and N. F. Ramsey, Phys. Rev. **82**, 831 (1951).
[15] Cassels, Randle, Pickavance, and Taylor, Phil. Mag. **42**, 215 (1951).
[16] Cladis, Hess, and Mayer, Phys. Rev. **87**, 425 (1952).
[17] Goodell, Loan, and Durbin, Phys. Rev. **83**, 234 (1951).
[18] Nelson, Guernsey, and Mott, Phys. Rev. **88**, 1 (1952).

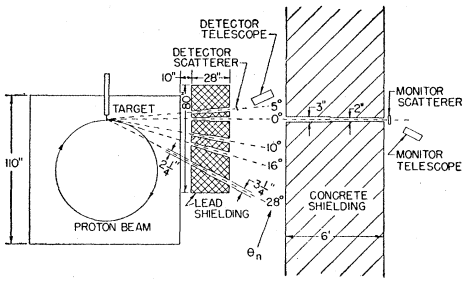

FIG. 1. Experimental arrangement indicating position of collimators, monitor and neutron spectrometer (detector).

incident 340-Mev proton beam. Observations of this type are restricted to such large angles because of the overwhelming Coulomb and diffraction scattering in the forward direction.

To observe the angular distribution of quasi-elastically scattered nucleons, it is therefore advantageous to utilize the large $n-p$ exchange scattering cross section. If a target is bombarded with protons and the neutrons produced in nucleon-nucleon type collisions are detected (or vice versa), observations can be made at all angles. The disadvantage of this method comes from the finite energy width of the primary beams which are intense enough to carry out the observations. Hadley and York[13] employed the 90-Mev neutron beam produced by deuteron stripping and detected protons, deuterons and tritons. Bodansky and Ramsey,[14] Cassels *et al.*,[15] Nelson *et al.*,[18] and Goodell *et al.*,[17] all placed their targets in a circulating proton beam and measured the energy spectrum of the ejected neutrons at one or at most, two angles. For a quantitative interpretation of certain of these results, the energy distribution of the internal beam must be known and this is difficult to measure accurately.

The interpretation of the angular distribution of high energy neutrons emitted from a cyclotron target should not require such an exact knowledge of the energy distribution of the primary beam. Using threshold detectors, Miller *et al.*,[19] DeJuren,[20] and Strauch[21] have measured such angular distributions. However, since both the energy response of the detectors and the energy distribution of the detected neutrons were largely unknown in these investigations, their quantitative interpretation was again quite difficult.

It was therefore decided to utilize a neutron spectrometer to measure the energy distribution of neutrons emitted from different targets at several angles with respect to the primary proton beam. The work reported here was carried out using the Harvard cyclotron at a radius corresponding to a nominal energy of 112 Mev. A later paper will report the results of a similar investigation carried out with protons with a nominal energy of 71 Mev. The neutron spectrometer and experimental method that were employed are described in some detail since they were used with little modification in the 71-Mev work and in other experiments still in progress in this laboratory. A short report on our results with Be and C targets has already been given.[22]

II. METHOD AND APPARATUS

(A) Experimental Arrangement

The targets were placed inside the cyclotron at a radius of 38.6 inches corresponding to a nominal beam energy of 112 Mev. The neutron spectrometer was situated between the tank and the concrete shielding (Fig. 1). This arrangement utilized as high a neutron flux as practicable (about 5×10^4 neutrons/cm^2/sec, with energy larger than 50 Mev with a Be target) and made possible measurements at various angles with respect to the proton beam without the necessity of any additional holes through the concrete shielding. The internal proton beam intensity was indirectly monitored by measuring the fast neutron flux with a proton recoil telescope placed outside the concrete shielding at 0° with respect to the internal proton beam. Physical dimensions are indicated in Fig. 1.

A lead block assembled with bricks collimated the neutrons emitted from the internal cyclotron target at angles of 0°, 5°, 10°, 16°, and 28° with respect to the proton beam. The neutron spectrometer was of standard design. A counter telescope detected and measured the energy of recoil protons emitted at 20° from a scatterer placed in one of the collimated neutron beams (Fig. 2). By the alternate use of polyethylene and carbon scatterers, those protons originating in $n-p$ collisions only could be obtained from the CH_2-C difference. The counting system recorded, simultaneously, the number of protons stopping in crystals *D*, *E* and *F*. The 50–112-Mev neutron energy range was covered by inserting up to 4 carbon absorbers into the telescope. As shown in Sec. E, the resulting proton differential range spectrum was converted to a neutron energy spectrum by using the known $n-p$ scattering cross sections.

At each of the five angles of observation, positioning rails were permanently installed for the spectrometer

TABLE I. Dimensions of scatterers and crystals.

	Area (cm²)	Thickness (g/cm²)
CH_2 scatterer	3.81×3.81	0.592
C scatterer	3.81×3.81	0.720
Crystal *A*	2.82×4.33	0.485
B	2.61×3.57	0.400
C	1.92×3.01	0.456
D	1.63×2.65	0.401
E	2.59×4.27	0.348
F	2.68×4.32	0.358
G	3.02×4.23	0.428

[19] Miller, Sewell, and Wright, Phys. Rev. **81**, 374 (1951).
[20] J. DeJuren, Phys. Rev. **81**, 458 (1951).
[21] K. Strauch, Phys. Rev. **82**, 299 (1951).
[22] K. Strauch and J. A. Hofmann, Phys. Rev. **86**, 563 (1952).

telescope and scatterer holder. This allowed a rapid shift from one angle to another with good reproducibility. An automatic target changer was used to interchange CH_2 and C scatterers by remote control.

The three-crystal monitor telescope used in this work was originally constructed by Bodansky and Ramsey.[14] It was placed outside the cyclotron shielding (Fig. 1) in a region of low background so that a slow (10^{-6} sec) coincidence circuit could be used. The telescope detected protons emitted from a 1-inch thick polyethylene scatterer and its counting rate was such as to contribute little to the statistical uncertainty of the points obtained with the neutron spectrometer.

The spectrometer telescope consisted of seven stilbene scintillation counters. Each crystal was about 0.125 inch thick and was held in place by a Lucite frame, which also served as a short light pipe to the photomultiplier. A 0.001-inch aluminum reflector surrounded the crystal assembly. The 1P21 photomultipliers were enclosed in iron shields to minimize the effect of the stray magnetic field from the cyclotron (about 50 gauss). The effect of this field on the path of the recoil protons can be neglected.

The dimensions of the scatterers and crystals are given in Table I. The dimensions of the scatterer and crystal D define the solid angle within which protons from the scatterer were accepted. All other crystals were larger than necessary to cover this solid angle in order to minimize the effect of proton scattering and of crystal positioning. For the same reason, all counters except A were placed as close together as it was physically possible. The final geometry was checked by obtaining the same points of a neutron energy spectrum alternately with crystals D, E, and F. Within 4 percent statistics, no significant difference was observed.

The recoil protons could also scatter in the absorbers. This possible source of error was minimized by using carbon absorbers with dimensions much larger than crystal D and by placing them close to this crystal. When the absorbers were moved next to crystal A, no significant change in counting rate occurred and it is therefore concluded that the elastic scattering of recoil protons in the absorbers could be neglected. The effect of nuclear absorption and inelastic scattering will be considered in Sec. G.

Not all the protons detected by the counter telescope originated in the scatterers, but about 25 percent were produced at the edges of the collimator, in the first crystal and in air. The effect of these background protons was eliminated by the subtraction indicated in Sec. E.

TABLE II. Spectrometer resolving power *vs* neutron energy.

Half-width from	55 Mev	90 Mev
(1) Thickness	9.2 Mev	6.4 Mev
(2) Angle	3.1 Mev	5.0 Mev
(3) Scattering	1.4 Mev	1.8 Mev
Total	9.8 Mev	8.3 Mev

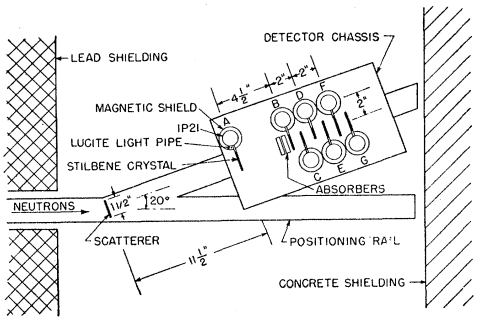

FIG. 2. The neutron spectrometer showing position of scatterer, counters, and absorbers.

The polyethylene and carbon scatterers were of equal stopping power. Before each run they were carefully aligned with respect to the counter telescope. Tests showed that the scatterer position was not very critical.

(B) Resolving Power

The uncertainty in the neutron energy measured by the spectrometer described in the previous section depends primarily on the following three factors:

(1) The range of the recoil proton is only defined within the thicknesses of the scatterer and the stopping crystal.

(2) The collision angle between neutron and proton varies around 20° due to the finite area of detector and defining crystal.

(3) An additional uncertainty in the $n-p$ collision angle is introduced by multiple scattering in the scatterer.

Table II shows the contribution of these factors to the spectrometer resolving power for 50-Mev and 90-Mev neutrons. The calculations are carried out using the thickness and largest width of crystal D. The half-widths of Table II refer to the full width at the half-intensity point. The resolution curves corresponding to the three factors involved must be folded into each other by numerical integration. However, little error is made by assuming Gaussian shapes to compute the width of the final resolution curve and the results quoted in Table II were obtained by this procedure.

It is seen from Table II that the geometry used in the spectrometer leads to comparable resolving power at the upper and lower limit of the neutron energy spectrum covered. This is the result of compensating effects in the energy dependence of the three factors involved.

(C) Recording Equipment

The individual peak counting rate in each crystal was of the order of 4×10^4 counts per second. Most of these counts resulted from knock-on protons produced in the crystals by the large neutron flux inside the cyclotron shielding. Since the overwhelming majority

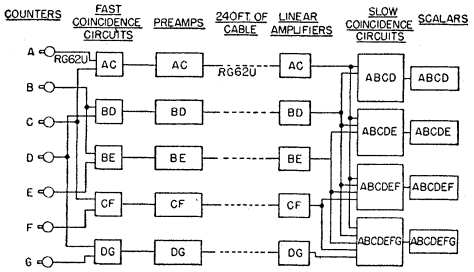

FIG. 3. Block diagram of recording equipment.

of neutrons reaching the counters have undergone one or more scatterings, the average energy of these neutrons is lower than that of the primary beam.

The protons coming from the scatterer produced, at most, a peak counting rate in each counter of 4×10^2 counts per second. This means that the main difficulty in the use of the counter telescope so close to the cyclotron tank came from the possibility of a large number of accidental coincidences contributing appreciably to the observed coincidence counting rate. Because of space limitation, it would have been difficult to better shield the counters from scattered neutrons and thus to reduce the single counting rate. Instead, a coincidence system with a resolving time of $1\text{–}2\times10^{-8}$ sec was used.

This system is described in detail elsewhere.[23] It utilized a "fast" coincidence circuit of the bridge type which registered twofold coincidences only. As shown in Fig. 3, five such circuits were used to make *AC*, *BD*, *BE*, *CF*, and *DG* coincidences. The bridge outputs were amplified to about 1.5 v before being transmitted to the counting room. There they were amplified still further and applied to "slow" coincidence circuits with resolving times of about 0.5×10^{-6} sec.

To increase the stability of the electronic system and to minimize the number of accidental coincidences, the fourfold *ABCD* coincidence was the lowest order coincidence observed. The thickness of the first three crystals thus determined the lowest energy proton that could be detected. After it was learned how to adjusr the components of the fast coincidence circuits fot optimum performance for the particular conditions encountered in this work, good plateaux were obtained for all of the photomultiplier high voltages and the amplifier gains, as shown in more detail in reference 23.

Since the photomultiplier output pulses were fed directly into the coincidence circuit, no counts were expected to be lost due to dead time effects in the electronic circuits. That this indeed was the case was shown by the independence of normalized counting rates on proton beam intensity.

Careful measurements showed that accidental coincidences and single pulse feed-through added at most 3 percent to the apparent number of protons stopping in a crystal, and this contribution was usually much smaller. It was therefore neglected in the results reported in Part III. During the long experimental runs, frequent checks were made to insure the the contribution from accidentals to the total counting rate remained negligible.

[23] K. Strauch, submitted to the *Review of Scientific Instruments*.

(D) Calculation of the Neutron Spectra

Only protons originating in $n-p$ collisions can be used to reconstruct the neutron energy spectra from the proton range spectra observed with the spectrometer telescope. Using the scatterers described in Table I, the number of recoil protons N_H is obtained from the following subtraction:

$$N_H = N_{CH_2} - 0.705N_C - 0.295N_b,$$

where N represents the number of protons detected by the telescope per monitor count and the subscripts identify the origin of the protons: hydrogen (H), polyethylene (CH_2), carbon (C), and background (b). The coefficient 0.705 is the ratio between the number of atoms per cm^2 of carbon in the CH_2 target and the C target having the same stopping power for protons.

The average range of protons stopping in a given crystal was calculated from the amount of material present between the centers of the scatterer and the stopping crystal using the tables of Aaron *et al.*[24] To obtain the differential range spectrum, the number of protons stopping in a given crystal was divided by its thickness, since crystals *D*, *E*, and *F* had different thicknesses.

The conversion of the differential proton range spectrum into the corresponding neutron energy spectrum was carried out as follows: (1) A proton energy spectrum was first calculated. The energy E_p corresponding to a given range R was obtained from the tables of Aaron *et al.*[24] The number of protons of energy E_p was then

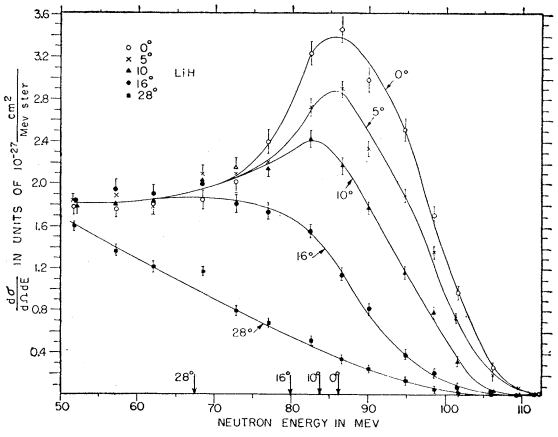

FIG. 4. Energy distribution of neutrons emitted from the LiH target at several angles θ_n with respect to the direction of the incoming proton beam. Arrows indicate the energies corresponding to 86 $\cos^2\theta_n$ Mev.

[24] Aaron, Hoffman, and Williams, U. S. Atomic Energy Commission Report AECU-663 (unpublished).

divided by the rate of energy loss dE/dx of these protons in stilbene. This division was necessary since the number of protons of range R that stop in a crystal is proportional to the range interval ΔR defined by the crystal. As long as $\Delta R \ll R$, this range interval is proportional to the dE/dx of protons of energy corresponding to the range R. (2) The conversion efficiency of the scatterer is proportional to the differential $n-p$ cross section at 20° which is energy dependent. The proton energy spectrum was thus divided by the differential $n-p$ cross section at the corresponding neutron energy E_n. The differential $n-p$ cross section values were interpolated from the results of Hadley *et al.*[25] for the angular distribution and from the data of Taylor *et al.*[26] for the total cross section.

The results of these calculations then represented the energy spectrum of neutrons emitted from the cyclotron target.

(E) Proton Beam Energy Distribution

As seen by an internal target, the cyclotron proton beam is not monoenergetic but has an appreciable energy spread. Evidence will now be presented to show that the proton energy half-width is of the order of 20 Mev with the LiD and Be targets used in this work. According to Gluckstern-Bethe,[27] and Chew,[28] high energy monoenergetic protons incident on a thin D target will produce neutrons which, when emitted in the forward direction, have an energy spread of about 1.5 Mev only. As shown in Fig. 11, we have observed a half-width of 22 Mev in this experiment. Thus, we believe that the 0° spectrum in Fig. 11 represents quite well the energy distribution of the internal proton beam, except that the energy scale should be increased by about 4 Mev to compensate for the energy lost in the target and the threshold of the observed reaction. This is supported by the very similar shape of the 0° Be −0.76C peak (Fig. 14) which is interpreted as being due to the scattering of protons by the loosely bound neutron in Be^9.

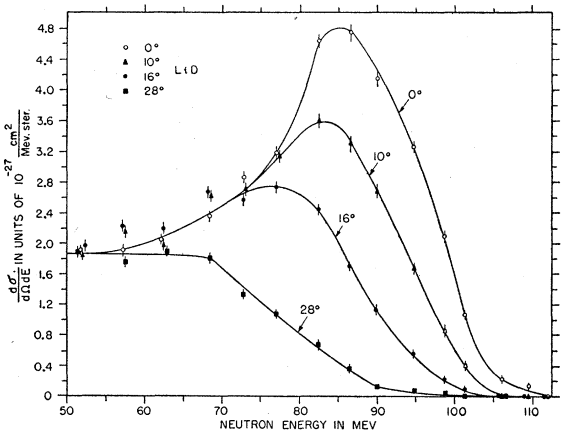

FIG. 5. Energy distribution of neutrons emitted from the LiD target at several angles.

TABLE III. Target dimensions.

Target	Height cm	Width cm	Thickness g/cm²	dE/dx (95 Mev) Mev	$\langle\theta^2\rangle_{Av}^{\frac{1}{2}}$ degrees
LiH	3.84	1.244	0.437	3.32	0.45
LiD	3.85	1.244	0.474	3.20	0.44
Be	4.45	0.635	0.584	3.76	0.61
C	4.45	0.635	0.776	5.35	0.89
Al	4.45	0.635	1.328	7.95	1.61
Cu	4.45	0.635	1.610	8.10	2.44
Pb	4.45	0.635	1.879	6.85	3.84

Two factors are believed to be mainly responsible for energy spread: (1) radial oscillations and (2) energy loss and scattering in the target during the first and subsequent traversals.

The amplitudes of the radial oscillations are a function of the operating conditions of the cyclotron and the beam energy distribution is thus a function of such variables as Dee high voltage, injection time, filament current and position, tank pressure, and others. Even with no change in the settings of the cyclotron controls, some of these variables will change slightly over 12-hour periods, and as a result the proton energy distribution changes slightly with time. To minimize the effect of these changes on our measurements, the data obtained with a given target were taken when stable operating conditions prevailed. The cyclotron was not shut down during a run in which a complete set of neutron spectra was obtained from a given target. However, the oscillator high voltage had to be turned off to change absorber or to move the spectrometer.

The importance of energy shifts during a run could be estimated from changes in the counting rate ratio of the spectrometer and monitor telescopes since these telescopes had different energy thresholds and sensitivities. The average energy of the internal cyclotron beam is believed not to have changed by more than 1 Mev during a set of measurements for one element. From run to run, energy shifts of up to 3 Mev could have occurred. The width of the 0° Be peak was found to remain constant within 15 percent during 3 runs spaced over a period of several months.

It would have been advantageous to use the method of Bloembergen and van Heerden[29] to measure the energy distribution of the internal beam for each of the targets employed. The installation of a magnetic channel inside the cyclotron tank, after the work of reference 29 had been completed, prevented such a program from being carried out. An estimate based on the energy loss and scattering angle of the protons in the various targets suggests that the energy spread of

[25] Hadley, Kelly, Leith, Segrè, Wiegand, and York, Phys. Rev. **75**, 351 (1949).
[26] Taylor, Pickavance, Cassels, and Randle, Phil. Mag. **42**, 328 (1951).
[27] R. L. Gluckstern and H. A. Bethe, Phys. Rev. **81**, 761 (1951).
[28] G. F. Chew, Phys. Rev. **84**, 710 (1951).
[29] N. Bloembergen and P. J. van Heerden, Phys. Rev. **83**, 561 (1951).

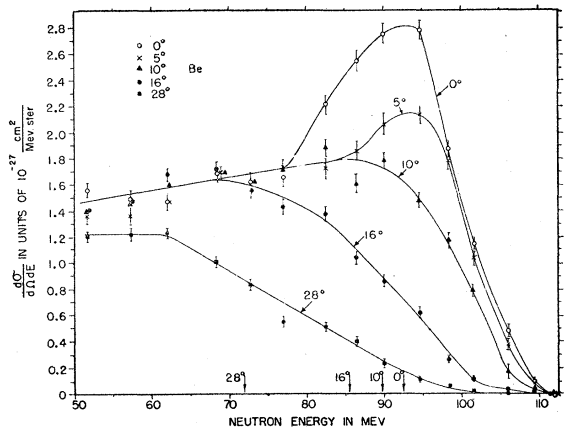

FIG. 6. Energy distribution of neutrons emitted from the Be target at several angles. Arrows indicate the energies corresponding to $92.5\cos^2\theta_n$ Mev.

the internal beam should not have been very different for the various targets.

(F) Measurement of Absolute Cross Sections

To determine the absolute cross sections to be assigned to the neutron energy distribution curves reported in Part III, it was necessary to measure the internal proton beam current. The following method was used for all targets except LiD. Two two-mil polystyrene foils were placed on each side of the target in question, in the manner of a sandwich. The target was then bombarded for about five minutes with the neutron counting equipment in operation and the *ABCD* telescope counts were noted. The absolute amount of C^{11} formed in each of the foils by the $C^{12}(p, pn)C^{11}$ reaction was then determined by measuring the annihilation radiation of the 20.5-minute activity of C^{11} with a calibrated Geiger counter.[30] The use of two foils on each side of the target allowed for the difficulty in lining up (1) the edges of the four foils flush with the inner edge of the target and (2) the inner edge of the target tangential to the orbit of the incident proton beam. The average of the activities of the four foils was taken to be the best value.[31] No distortion in foil activities due to nucelar recoils was noticed.

To arrive at the cross section for the formation of C^{11} in the foils, the experimentally known $C^{12}(p, pn)C^{11}$ excitation function[32] had to be averaged over the energy distribution of the incident proton beam. A good approximation to this distribution was believed to be the 0° neutron energy distribution of D (see Sec. *H*). The corresponding average cross section for the formation of C^{11} thus calculated was 78.6 mb, and was the value used in the absolute cross-section computations for all targets.[33] The differences in the proton energy distributions for the various targets, due to differences in stopping power and scattering, are believed to lead to less than 10 percent variation in the cross section for C^{11} formation. An additional estimated 5 percent uncertainty is introduced by the fact that the neutron energy distribution measurements and the corresponding absolute cross-section measurements were made at different times.

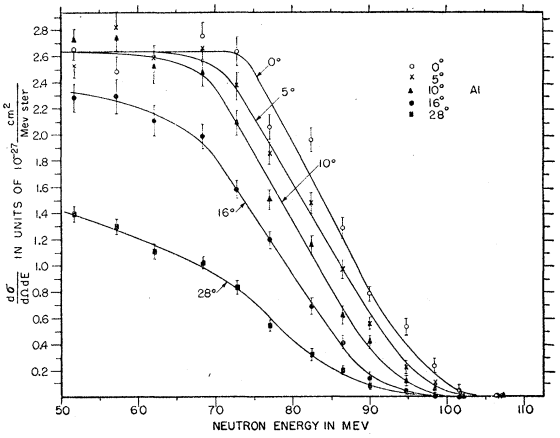

FIG. 8. Energy distribution of neutrons emitted from the Al target at several angles.

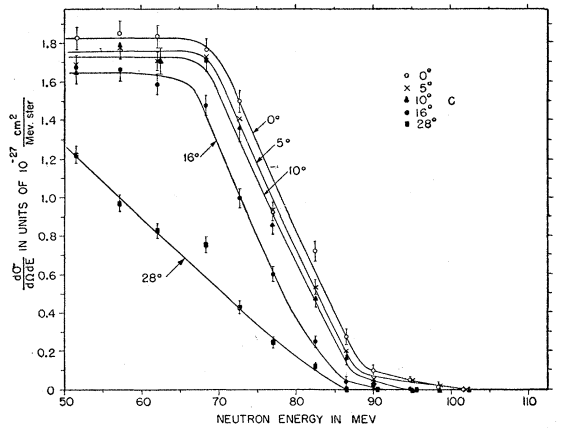

FIG. 7. Energy distribution of neutrons emitted from the C target at several angles.

[30] Two standards were used to calibrate the Geiger counter: (1) a polystyrene foil (of the same dimensions as those used with the targets) whose absolute C^{11} activity was determined by a $\beta-\gamma$ coincidence method; (2) a RaD—RaE source calibrated by the National Bureau of Standards. The two independent methods of calibration agreed within 5 percent and the average value was taken as the true efficiency.

[31] The foil activity is proportional to the total integrated proton beam current passing through the target and hence includes the effect of multiple traversals.

[32] N. M. Hintz and N. F. Ramsey, Phys. Rev. 88, 19 (1952).

[33] If one takes the 0° neutron energy distribution of Be—0.76C (Fig. 14) to represent the correct internal proton beam distribution, one obtains an average cross section of 75.4 mb. For the heavier targets such as Pb, the average cross section is probably higher than 78.6 mb, but we do not know how to make a good estimate. As a result, no attempt has been made to use a different effective cross section for each target, and the value used is believed to represent a fair average.

Three complete determinations were made of the absolute cross section for each target investigated and the average taken as the final value.

To obtain the cross section for the LiD target, the LiD and LiH targets were mounted on the same target probe. By alternately rotating these targets into the proton beam for short intervals of time, the relative neutron yield was measured and beam variations averaged out. A 4 percent correction was applied to the experimental ratio to compensate for the difference in the number of Li atoms in the two targets. Since the cross section for neutron production from LiH was measured by the standard method, the corresponding result for LiD and D could be easily calculated.

The measured cross sections were increased by 17±6 percent to compensate for neutron absorption and scattering in the cyclotron wall and nuclear proton absorption in the telescope.

On the basis of the above discussion, an estimate of the over-all uncertainty in the accuracy of our absolute cross sections is 25 percent.

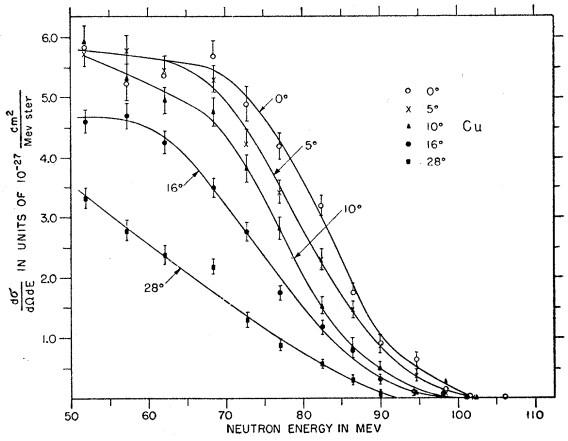

FIG. 9. Energy distribution of neutrons emitted from the Cu target at several angles.

III. MEASUREMENTS AND RESULTS

The energy spectrum of neutrons emitted from LiH, Be, C, Al, Cu, and Pb targets was measured at angles[34] of 0°, 5°, 10°, 16°, and 28° and from a LiD target at 0°, 10°, 16°, and 28°. The LiH and LiD targets were placed at a radius of 38.1 inches (nominal beam energy of 109 Mev). All other targets were located at a radius of 38.6 inches (nominal beam energy of 112 Mev).

Table III lists the dimensions, energy loss, and scattering angle $\langle\theta^2\rangle_{Av}^{\frac{1}{2}}$ for 95-Mev protons of the various targets (assuming 1 traversal). The targets were held in place by two light clips 1.25 inches long which were attached to a long probe (Fig. 1). Geometrical considerations indicate that the number of high energy neutrons produced in the probe that could have entered the collimating channel was negligible.

[34] Due to multiple scattering of the proton beam in the cyclotron targets, the neutrons observed in the geometrical 0° direction are actually emitted at small angles of the order of one-half of the root mean square scattering angle $\langle\theta^2\rangle_{Av}^{\frac{1}{2}}$ indicated in Table III.

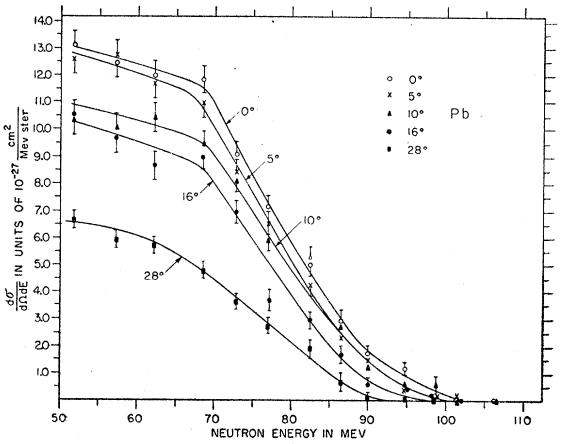

FIG. 10. Energy distribution of neutrons emitted from the Pb target at several angles.

About 7 hours of running time were needed to obtain the spectrum from one element at one angle.

The results of these measurements are plotted in Figs. 4–10. Figure 11 represents the neutron spectrum from D and was obtained by subtraction of the LiH from the LiD results. Indicated errors are from statistics only.

Our results fall into three groups:

(1) The number of neutrons emitted by C, Al, Cu and Pb targets decreases with neutron energy.

(2) The energy distribution of neutrons emitted from D is peaked and its shape is believed to represent the energy distribution of the primary proton beam.

(3) Neutrons emitted from Li and Be show a peaked energy distribution, with the size of the peak decreasing rapidly with increasing emission angle.

IV. DISCUSSION AND INTERPRETATION

(A) C, Al, Cu, and Pb Targets

Goldberger[6] has performed calculation on the interaction of 90-Mev neutrons with a Pb nucleus. He has

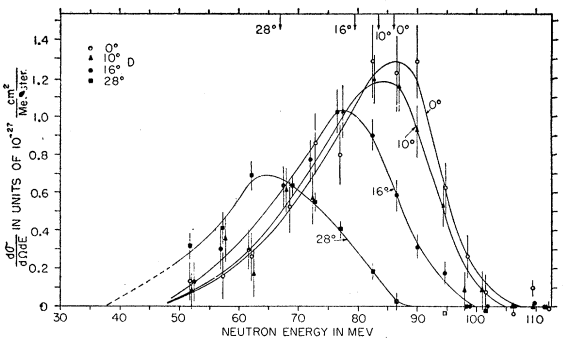

FIG. 11. Energy distribution of neutrons emitted from D as obtained by the LiD—LiH subtraction. Arrows indicate the energies corresponding to 86 $\cos^2\theta_n$ Mev.

TABLE IV. Relative angular distributions.

Target \ θ_n	0°	5°	10°	16°	28°
	All neutrons with $E_n>70.7$ Mev				
Li	1.00	0.85	0.68	0.41	0.15
Be	1.00	0.85	0.68	0.44	0.16
C	1.00	0.89	0.81	0.53	0.23
Al	1.00	0.81	0.63	0.44	0.21
Cu	1.00	0.85	0.63	0.44	0.20
Pb	1.00	0.86	0.88	0.59	0.38
	All neutrons with $E_n>65.9$ Mev				
Li	1.00	0.88	0.72	0.49	0.20
Be	1.00	0.87	0.72	0.51	0.22
C	1.00	0.93	0.88	0.64	0.30
Al	1.00	0.85	0.70	0.51	0.25
Cu	1.00	0.85	0.69	0.50	0.26
Pb	1.00	0.88	0.85	0.65	0.39
	All neutrons with $E_n>48.6$ Mev				
Li	1.00	0.92	0.80	0.63	0.35
Be	1.00	0.89	0.80	0.63	0.36
C	1.00	0.93	0.91	0.78	0.45
Al	1.00	0.93	0.85	0.67	0.36
Cu	1.00	0.94	0.84	0.66	0.39
Pb	1.00	0.94	0.83	0.72	0.44
	All neutrons with $E_n>65.9\cos^2\theta_n$ Mev				
Li	1.00	0.89	0.77	0.60	0.44
Be	1.00	0.88	0.76	0.62	0.45
C	1.00	0.97	1.02	0.98	0.93
Al	1.00	0.87	0.80	0.72	0.61
Cu	1.00	0.88	0.80	0.73	0.71
Pb	1.00	0.92	0.98	0.91	0.91
	Free $N-P$ scattering[25,41]				
	1.00	0.95	0.78	0.65	0.43

obtained the energy and angular distribution of protons emerging at all angles immediately after bombardment, before evaporation takes place. These results can be summarized as follows:

(1) Protons with energies up to the maximum value allowed by threshold considerations are emitted, with a small peak in the energy spectrum at high energy.

(2) There is a minimum in the angular distribution of high energy protons in the forward direction, since small momentum transfers are forbidden by the exclusion principle.

It is believed that the equality of $n-n$ and $p-p$ forces holds in the high energy region.[27,28] This means that Goldberger's predictions apply equally well to the work reported here where protons interacted with the target nucleus, and neutrons were detected. The only difference between this and the inverse experiment arises from the unequal number of neutrons and protons in the target nucleus. This fact will mainly affect the absolute cross sections, not the angular and energy distributions.

As a matter of fact, our observations are much more detailed than the predictions of the available calculations based on the Goldberger model. The labor involved in carrying out the calculations to much higher accuracy would probably be excessive.

As seen in Figs. 4–11, a considerable number of high energy neutrons are emitted. It is somewhat surprising that no high energy peak appears to exist in the forward direction especially at least for the lighter elements.[35] According to Fernbach,[5] the mean free path in nuclear matter for 90-Mev neutrons is 3.3×10^{-13} cm, which should be compared to the radius of C(3.2×10^{-13} cm) and of Al(4.2×10^{-13} cm). Our results on the shape of the energy spectrum are in agreement with those of Hadley and York[13] who performed the inverse experiment with 90-Mev neutrons.

The effect of the exclusion principle, as applied in the Goldberger model, is of course such as to reduce the number of high energy neutrons. We do not believe that this is the entire explanation for the absence of a peak in the 100-Mev region for two reasons. When protons with an average energy of about 150 Mev are used, peaks are observed at 2.5° in the neutron energy distribution even in a heavy nucleus such as U.[15] It is not clear how the effect of the exclusion principle could show such a drastic energy dependence, without a corresponding strong dependence on the atomic number. Secondly, the angular distributions observed in this work do not agree with those predictions of the Goldberger model which are directly related to the role of the exclusion principle.

It also does not seem very probable that the increased mean free path in nuclear matter at the higher proton energy can explain the difference between the 95-Mev and 150-Mev results, if it is assumed that the cross section for nucleon-nucleon collisions inside the nucleus has the same energy dependence as free collisions. Between 97 and 156 Mev, the total $n-p$ cross section[26] decreases by a factor of 1.59 ± 0.08[36] while from C to U, the radius increases by a factor of 2.59. Thus, since a significant neutron peak is observed when protons with an average energy of 150 Mev are used with U,[15] it would seem reasonable from these considerations to expect a neutron peak from C when bombarded with 95-Mev protons.

That these general arguments do not qualitatively explain the observations on the shape of the neutron spectra is not too surprising if it is remembered that the optical model apparently fails to predict the rapid decrease of the total neutron scattering cross section that occurs for most elements between 70 Mev and 150 Mev.[37] It might well be that a future explanation for the rapid increase of the nuclear transparency in this energy region will also explain the difference in neutron spectra observed with 95-Mev and 150-Mev protons.

The minimum in the forward direction in the angular distribution which was predicted by Goldberger is not

[35] Goldberger's energy spectrum (reference 6) of the particles emitted at all angles predicts the existence of such a peak for 90-Mev neutrons incident on Pb.

[36] This number represents an upper limit only to the corresponding ratio of the differential cross sections in the forward direction.

[37] J. DeJuren and B. J. Moyer, Phys. Rev. **81**, 919 (1951).

observed. It has been suggested that refraction at the nuclear surface of the incoming and outgoing particle wave might wash out this minimum. Meadows[38] has performed a Goldberger type of calculation which includes the effect of refraction for the case of Cu bombarded by 100-Mev protons. His results still show a pronounced dip in the number of neutrons emitted in the forward direction.

If secondary collisions are more important than predicted by these calculations which are based on the free nucleon-nucleon interaction cross sections, then the minimum might be washed out. Such an effect might also explain the absence of a peak in the neutron energy distribution from C and the heavier targets. Before concluding that the Goldberger model itself is at fault, it would be instructive to measure angular distributions at higher energies where the energy spectra correspond more closely to the theoretical predictions.

Table IV can be used to compare the angular distributions from the various targets with each other and with that of free neutron-proton collisions. Columns I, II, and III give the relative angular distribution of all neutrons with energies above 70.7 Mev, 65.9 Mev, and 48.6 Mev, respectively. As the cut-off energy is decreased, the forward peak becomes broader indicating the increased contribution of neutrons involved in secondary collisions. With the 65.9-Mev and 70.7-Mev cut-off energies, the angular distribution decreases faster than the free neutron-proton differential cross section.

This result is not surprising since a cut-off energy of $E_0 \cos^2\theta_n$ should be used if the target nucleons were free and no secondary collisions occurred. In column IV of Table IV is listed the relative angular distribution of all neutrons with energies larger than 65.9 $\cos^2\theta_n$ Mev. With this energy limit, the angular dependence is less peaked than that of free $n-p$ collisions, indicating the importance of the internal momentum distribution of the target nucleons and the effect of multiple collisions.

This last factor probably explains the observation that the angular distribution of the neutrons emitted from Pb is less peaked than that obtained from Al and Cu. The broadest angular peak is observed with a C target for which the role of multiple collisions should be smallest. This apparent anomaly is probably connected with the very high threshold (18.7 Mev) of the (p, n) reaction for this element. Only those neutrons can escape the C nucleus, which have been created in a collision in which at least 18.7 Mev has been transmitted to the remainder of the nucleus. Collisions in which only small momenta are transferred are therefore suppressed, and it is just those collisions that contribute to the forward emission of high energy neutrons. The anomalous behavior of C had been observed previously.[21]

The measured cross sections for the production of neutrons with energies larger than 48.6 Mev from C, Al, Cu, and Pb targets are proportional to $A^{\frac{2}{3}}$. This dependence is shown both by the differential cross section in the forward direction and by the inelastic cross section integrated up to 28° as can be seen in Fig. 12. An $(A-Z)^{\frac{2}{3}}$ dependence previously found by Knox[39] with 340-Mev protons or an $(A-Z)/A^{\frac{1}{3}}$ dependence as suggested by Mandl and Skyrme[40] would also be in agreement with our results.

(B) Deuterium

The high energy neutron-deuteron interaction has been discussed by Gluckstern and Bethe[27] and by Chew.[28] Their calculations on the yield of high energy protons are directly applicable to our results on the inverse reaction.

Since the deuteron has such a loosely bound structure and its wave function has relatively few high momentum components, these authors show that if high energy monoenergetic protons were incident on a deuterium target, high energy neutrons would be emitted in the forward direction with an energy spread of the order of only 1.5 Mev. These neutrons are identified as the products of an exchange-type $n-p$ collision where the target neutron is in the deuterium nucleus. As shown in detail by Chew using the impulse approximation, the yield and angular distribution of the high energy protons is different from that expected from free $n-p$ collisions mainly because of the exclusion principle. For if a high energy neutron is emitted in the forward direction, little momentum has been left to the incident proton which may then find itself in a region of phase space already occupied by the second proton.

Our results for D are shown in Fig. 11. It is apparent that the neutron energy width of 22 Mev is considerably larger than expected from the theory and the energy resolution of our apparatus (Part II). This we believe to be due to the inherent energy spread of the

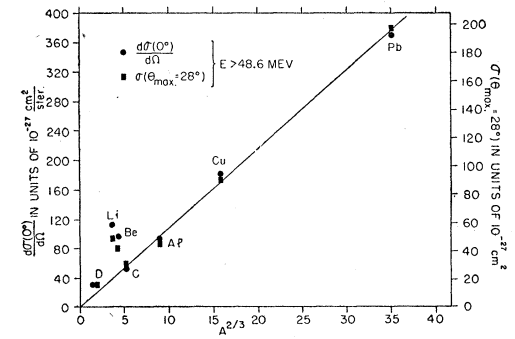

FIG. 12. Plot of the differential cross sections in the forward direction $d\sigma(0°)/d\Omega$ and the cross sections σ (integrated up to $\theta_n=28°$) against $A^{\frac{2}{3}}$. These cross sections refer to the production of neutrons with energies larger than 48.6 Mev by protons centered around 95 Mev.

[38] J. Meadows (private communication).

[39] W. J. Knox, Phys. Rev. **81**, 687 (1951).

[40] F. Mandl and T. H. R. Skyrme, Atomic Energy Research Establishment (Harwell) Report No. TR745 (unpublished).

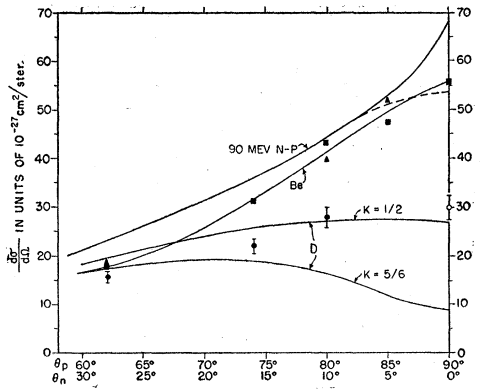

FIG. 13. Comparison of the free $n-p$ scattering cross sections in the laboratory system with the neutron yields from D and from the loosely bound neutron in Be. The full $n-p$ cross section curve summarizes the data of Hadley *et al.* (reference 25), while the dotted portion gives more recent results of Selove, Strauch, and Titus (private communication). Two independent measurements of the angular distribution of neutrons emitted by Be are reported using the symbols ▲ and ■. The D curves refer to theoretical results of Chew (see text).

primary proton beam, and this interpretation is compatible with the measurements of Bloembergen and van Heerden.[29] The peak width is thus of no interest as far as the theory of proton-deuteron scattering is concerned. However, the position of the peak varies as $E_0 \cos^2\theta_n$ where E_0 is the energy at the maximum of the 0° peak as expected for a free neutron-proton collision, and the width of the peaks appears to remain constant with angle. This indicates that within our experimental accuracy the kinematics of the $n-p$ interaction is not changed appreciably by the fact that the target nucleon is inside the D nucleus.

By integrating under the curves of Fig. 11, the differential cross section for the yield of high energy protons is obtained. The results are shown by the dots on Fig. 13 where the indicated errors are of statistical origin only. The area under the 28° curve has been multiplied by 1.07 to compensate for the neutron fraction below the threshold energy of our apparatus. Figure 13 also shows the free $n-p$ differential cross section at 90 Mev for comparison, and it is apparent that the effect of the exclusion principle is to reduce the neutron yield from deuterium.

According to Chew, this difference might be used as a measure of the spin dependence of the $n-p$ interaction although in the 90-Mev region such a conclusion is "optimistic." Be that as it may, we have also plotted on Fig. 13 the differential cross sections expected according to the calculations of Chew for the case $r_{1p^s} = r_{1p^t}$ ($K=\frac{1}{2}$) and $r_{1p^s}=0$ ($K=\frac{5}{8}$) (see reference 28 for nomenclature). Our results agree better with the $K=\frac{1}{2}$ curve.

Powell, as quoted by Chew,[28] has done the inverse experiment and his results seem to agree with ours within the respective experimental uncertainties.

The LiD−LiH subtraction is so unfavorable that it would be quite hard to improve the accuracy of our measurements. Instead, an experiment is in progress in this laboratory in which the yield of high energy protons from $n-$D scattering is directly compared to the free $n-p$ interaction cross section.

(C) Li and Be Targets

The neutron spectra observed with Li and Be targets (Figs. 4 and 6) are quite similar in that both exhibit a pronounced high energy peak in the forward direction whose height decreases rapidly with angle. The results must be contrasted with those obtained with the C target in which no such peaks occur (Fig. 7). The difference in peak energy between the 0° Li and Be results is explained by the higher threshold energy of the (p, n) reaction in Li (8.2 Mev) compared to Be (1.8 Mev) and by the fact that the Li bombardment was carried out at a slightly smaller radius (Part III).

It seems reasonable to attempt to explain observed spectrum differences between Li, Be, and C on the basis of the individual structure of these nuclei. In the case of Be^9, a model[41] which has been successful in explaining the results of low energy photodisintegration assumes that the loosely bound neutron (1.63 Mev) of Be^9 moves in the "effective field" of Be^8. Physically this means that this neutron spends a large fraction of its time outside the "inner core" composed of the Be^8 nucleus. The situation thus might be somewhat similar to the case of deuterium, so that the high energy peak observed with Be might correspond to those neutrons that have been produced in an exchange collision between the incoming proton and the loosely bound neutron of Be^9. The cross section for such a collision is expected to be quite similar to that for the free $n-p$ interaction in opposition to the case of D, since in the case of Be the exclusion principle is not expected to play an appreciable role.

That the loosely bound neutron plays a special role in the interaction of high energy protons with Be also follows from the anomalously high neutron yield observed with 95-Mev protons (Fig. 12) and 340-Mev protons.[39]

Be^8 is composed of two α-particles and thus should behave very much like the C^{12} nucleus as far as the production of high energy neutrons is concerned. For example, the Q values of the (p, n) reactions in C^{12} and Be^8 are −18.7 Mev and −18.8 Mev, respectively. A fair estimate of the contribution of Be^8 to the observed spectrum from Be^9 might thus be given by the C^{12} spectrum with the cross section multiplied by $(8/12)^{\frac{3}{2}}$ as suggested by the data summarized in Fig. 12. If this contribution is subtracted from the Be^9 spectra, the result shown in Fig. 14 is obtained.

[41] C. J. Mullin and E. Guth, Phys. Rev. **76**, 682 (1949).

The most striking feature of this result is the appearance of peaked neutron energy distributions at the five angles investigated. The width of the peaks increases with angle, but the energy of the maximum seems to follow the $E_0 \cos^2\theta_n$ law for free $n-p$ collisions as shown by the arrows on the abscissa of Fig. 14. The shape and width of the 0° Be−0.76C curve are quite similar to those obtained from D. This indicates that these features are again mainly determined by the energy distribution of the primary proton beam.

If our interpretation is correct, then the area under the curves of Fig. 12 represents the differential cross section for the scattering of the incident protons by the loosely bound neutron in Be^9. The validity of this assumption is supported by the fact that the 16° neutron spectrum from Be (Fig. 6) has a small maximum at about 70 Mev. After the contribution from Be^8 has been subtracted out, a peak appears at 85 Mev where it is expected for the simple model used. It does not seem very likely that such a coincidence is accidental.

The broadening of the peaks of Fig. 14 at the larger angles can be understood, at least qualitatively, by the fact that some of the outgoing neutrons will interact with the inner core of the Be nucleus. The lower the neutron energy, the more important this secondary interaction will become. The strong energy dependence of this effect is exemplified by decrease of the total neutron cross section of Be between 70 Mev and 90 Mev from 0.52 barn to 0.40 barn.

The differential cross sections obtained by integrating the area under the Be−0.76C curves has been plotted on Fig. 13. The points indicated by the triangles and squares represent the result of two independent measurements. It must be remembered that the absolute scale is only known to 25 percent. Within this relatively large uncertainty, it appears that the cross section for the 90° (laboratory system) scattering of protons by the loosely bound neutron in Be^9 is the same as in free $n-p$ collisions, but that at the smaller angles the cross section for the bound scattering decreases more rapidly than that of the free interaction. This behavior is probably due to the increasing importance of secondary collisions as also shown by the broadening of the neutron energy peaks.

The very simple model of the Be^9 nucleus that we have used to interpret our experimental data seems to lead to self-consistent results. How seriously it can be taken seems difficult to estimate at present. More information on the limits of validity of this model may result from an experiment on inelastic scattering of 100-Mev protons by the Be nucleus which is being planned in this laboratory.

The rapid decrease of the number of high energy neutrons emitted by Be between the angles of 0° and 16° leads to a very practical application. If it is desired to study the effect of high energy neutrons in an experiment such as production of stars in a photographic plate, simultaneous exposures can be made at 0° and 16°. A subtraction will then give the results produced by the high energy neutrons.

The neutron spectra observed with the LiH target (Fig. 4) are quite similar in shape to those obtained with Be but with a slightly larger cross section. Since natural Li is composed mainly of Li^7 (92.5 percent), most of the neutrons observed come from that isotope. It should not be possible in our energy region to use models for Li similar to those successful in the case of D and Be since the neutrons in Li are by no means loosely-bound—the binding energy in Li^7 is 7.15 Mev and in Li^6 is 5.17 Mev. That the height of the 0° Li peak is not twice the height of the Be peak, and that the yield of 50-Mev neutrons from Li is the same as that from Be (within the experimental error) is probably a result of the tighter binding of the outer shell neutrons in Li, the role of the exclusion principle as in D, and the possible difference in energy spectrum from the inner core of Li and Be.

(D) Summary

The neutron energy spectra observed from C, Al, Cu, and Pb targets when bombarded with 95-Mev protons seem in general qualitative agreement with the predictions of the theory of high energy nuclear reactions. However, the forward minimum in the angular distribution and a high energy peak in the energy distribution expected from calculations based on the Goldberger model have not been observed.

The neutron yield from D is of the order of magnitude predicted by Chew on the basis of his calculations with the impulse approximation. The yields clearly show the important role of the exclusion principle in the case of D.

The observations with Be have been interpreted on the basis of a simple model which gives the cross sec-

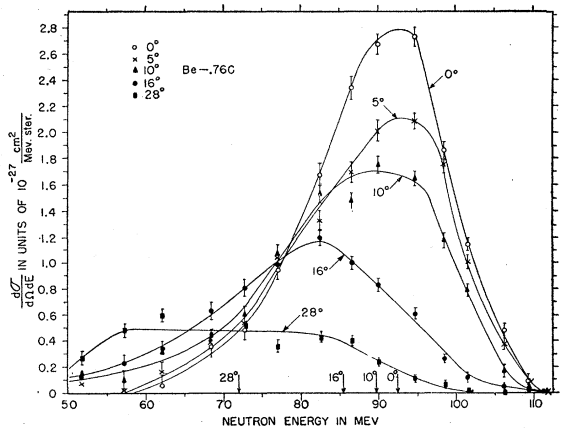

FIG. 14. Energy distribution of neutrons emitted by Be^9 after contributions from the "inner core" have been subtracted. Arrows indicate the energies corresponding to 92.5 $\cos^2\theta_n$ Mev.

tions for proton scattering with the loosely bound neutron in Be^9. If this model is correct, it can be stated within the experimental accuracy that the forward exchange scattering cross section for bound and free $n-p$ collisions are the same. It must be emphasized, however, that the loosely bound neutron in Be^9 is not necessarily representative of neutrons embedded in nuclear matter.

The authors wish to thank Professor N. F. Ramsey for his continuous and constructive interest. This investigation has been greatly assisted by the fine cooperation of the staff of the Cyclotron Laboratory.

PHYSICAL REVIEW VOLUME 90, NUMBER 3 MAY 1, 1953

The (α,n) and $(\alpha,2n)$ Cross Sections of Ag^{109}†

E. BLEULER, A. K. STEBBINS,* AND D. J. TENDAM
Department of Physics, Purdue University, Lafayette, Indiana
(Received January 19, 1953)

The excitation curves for the reactions $Ag^{109}(\alpha,n)In^{112}$ and $Ag^{109}(\alpha,2n)In^{111}$ have been measured for alpha-energies up to 19.5 Mev. The threshold for the $(\alpha,2n)$ reaction is 14.8 ± 0.2 Mev. The sum of the cross sections agrees approximately with the total cross section calculated for a radius $R\sim1.6\times10^{-13}A^{\frac{1}{3}}$ cm. The energy dependence of the ratio $\sigma(\alpha,2n)/\sigma(\alpha,n)$ can be interpreted as being in agreement with either a nearly constant nuclear temperature of 1.7 Mev or with a level density $\omega(E)=\text{const}\exp[2(aE)^{\frac{1}{2}}]$ with $a=2.5$ Mev^{-1}. The corresponding temperature $\Theta=(E/a)^{\frac{1}{2}}$ varies from 1.7 Mev to 2.2 Mev for excitation energies between 7.5 and 12 Mev. These apparent temperatures are considerably higher than those found by direct measurement of (p,n) and (n,n) neutron spectra.

I. INTRODUCTION

ACCORDING to the theory of nuclear reactions, as developed on the basis of the Bohr assumption, the determination of the relative cross sections for primary and secondary reactions can furnish information about the level spacing for intermediate and heavy nuclei.[1,2] Consider the reactions $Ag^{109}(\alpha,n)In^{112}$ and $Ag^{109}(\alpha,2n)In^{111}$. The energy distribution of the primary neutrons is given by

$$I(\epsilon)d\epsilon=\text{const}\,\epsilon\sigma_C(\epsilon)\omega(\epsilon_{\max}-\epsilon)d\epsilon, \quad (1)$$

where $\sigma_C(\epsilon)$ is the cross section for the formation of the compound nucleus In^{113} from the level of the residual nucleus In^{112} reached in the reaction. If $\sigma_C(\epsilon)$ is known from the theory the level density ω of In^{112} at an excitation energy $E=\epsilon_{\max}-\epsilon$ can be computed directly from the measured intensity distribution $I(\epsilon)$. The measurement of neutron spectra, however, is rather tedious and, for higher excitation energies, made uncertain by the emission of secondary neutrons. Relative cross sections, on the other hand, can be determined by simple activity measurements. Assuming that a second neutron is evaporated whenever it is energetically possible, one obtains for the cross-section ratio

$$r(\epsilon_\alpha)=\sigma(\alpha,2n)/\sigma(\alpha,n)=\int_0^{\epsilon_{\max}-S}I(\epsilon)d\epsilon\Big/\int_{\epsilon_{\max}-S}^{\epsilon_{\max}}I(\epsilon)d\epsilon. \quad (2)$$

Here, ϵ_α is the initial kinetic energy in the c.m. system, i.e., essentially the alpha-energy. S is the separation energy of the second neutron from In^{112}, $\epsilon_{\max}-S=\epsilon_\alpha-T_{2n}$ the maximum energy a primary neutron can have without making the escape of a secondary neutron impossible. T_{2n} is the threshold energy for the $(\alpha,2n)$ reaction.

It is obvious that the level density $\omega(E)$ is not determined uniquely by (2), even if the cross-section ratio is known as a function of ϵ_α. Neglecting the variation of $\sigma_C(\epsilon)$ one obtains, for $E=S+\epsilon_\alpha+T_{2n}$,

$$\omega(E)=\text{const}\left\{\frac{d^2r}{d\epsilon_\alpha{}^2}+B\left[2\frac{dr}{d\epsilon_\alpha}+(\epsilon_\alpha-T_{2n})\frac{d^2r}{d\epsilon_\alpha{}^2}\right]\right\},$$

with

$$B=\int_0^S\omega(E)dE\Big/\int_0^S dE\int_0^E\omega(E')dE'.$$

Since B is not known, no direct calculation of $\omega(E)$ is possible. Instead, the measurements are used to determine the parameter in some assumed level density function, e.g., the nuclear temperature Θ. By developing the logarithm of the level density in the neighborhood of $\epsilon_{\max}$, using $d(\ln\omega)/dE=1/\Theta$, one can approximate Eq. (1) by $I(\epsilon)=\text{const}\,\epsilon\sigma_C(\epsilon)e^{-\epsilon/\Theta}$. Assuming $\sigma_C(\epsilon)=\text{const}$, and $\epsilon_{\max}\gg\epsilon_{\max}-S$, the cross-section ratio becomes

$$r(\epsilon_\alpha)=\sigma(\alpha,2n)/\sigma(\alpha,n)=e^x/(1+x)-1=f(x), \quad (3)$$

with $x=(\epsilon_\alpha-T_{2n})/\Theta$.

Theoretical estimates of the dependence of Θ on E vary with the model used. Blatt and Weisskopf[2] give, for a degenerate-gas model, $\Theta=(E/a)^{\frac{1}{2}}$, which leads to

† Work supported by the U. S. Office of Naval Research and the U. S. Atomic Energy Commission.
* Now at U. S. Military Academy, West Point, New York.
[1] V. F. Weisskopf and D. H. Ewing, Phys. Rev. **57**, 472, 935 (1940).
[2] J. M. Blatt and V. F. Weisskopf, *Theoretical Nuclear Physics* (John Wiley and Sons, Inc., New York, 1952), Chap. VIII.